Assembly of Protein Complexes In and On the Membrane with Predicted Spatial Arrangement Constraints

Charles Christoffer[a], Kannan Harini[b,c], Gupta Archit[c,d] & Daisuke Kihara[a,c,e,*]

[a]Department of Computer Science, Purdue University, West Lafayette, IN, 47907, USA

[b]Department of Biotechnology, Bhupat and Jyoti Mehta School of Biosciences, Indian Institute of Technology Madras, Chennai 600036, India

[c]Department of Biological Sciences, Purdue University, West Lafayette, IN, 47907, USA

[d]Department of Genetic Engineering, SRM Institute of Science and Technology, Kattankulathur 603203, India

[e]Purdue University Center for Cancer Research, Purdue University, West Lafayette, IN, 47907, USA

[*]To whom correspondence should be addressed. Email: dkihara@purdue.edu Phone: +1 765-496-2284

ABSTRACT

Membrane proteins play crucial roles in various cellular processes, and their interactions with other proteins in and on the membrane are essential for their proper functioning. While an increasing number of structures of more membrane proteins are being determined, the available structure data is still sparse. To gain insights into the mechanisms of membrane protein complexes, computational docking methods are necessary due to the challenge of experimental determination. Here, we introduce Mem-LZerD, a rigid-body membrane docking algorithm designed to take advantage of modern membrane modeling and protein docking techniques to facilitate the docking of membrane protein complexes. Mem-LZerD is based on the LZerD protein docking algorithm, which has been constantly among the top servers in many rounds of CAPRI protein docking assessment. By employing a combination of geometric hashing, newly constrained by the predicted membrane height and tilt angle, and model scoring accounting for the energy of membrane insertion, we demonstrate the capability of Mem-LZerD to model diverse membrane protein-protein complexes. Mem-LZerD successfully performed unbound docking on 13 of 21 (61.9%) transmembrane complexes in an established benchmark, more than shown by previous approaches. It was additionally tested on new datasets of 44 transmembrane complexes and 92 peripheral membrane protein complexes, of which it successfully modeled 35 (79.5%) and 15 (16.3%) complexes respectively. When non-blind orientations of peripheral targets were included, the number of successes increased to 54 (58.7%). We further demonstrate that Mem-LZerD produces complex models which are suitable for molecular dynamics simulation. Mem-LZerD is made available at https://lzerd.kiharalab.org.

Keywords: protein structure prediction; protein-protein docking; membrane protein docking; membrane protein assembly

INTRODUCTION

Protein-protein interactions are fundamental to many biological processes in living cells. Membrane proteins play an essential role in many of these processes, where they act as gateways of cellular signaling pathways, pumps, and more, facilitating selective transport processes across membranes. To understand the detailed mechanisms of these processes, modeling the 3D structures of their associated protein complexes is a critical step. While protein complex structures are steadily being determined by experiment and deposited in the Protein Data Bank (PDB) [1, 2], experiments are still expensive and a substantial human and instrument time investment, assuming the proteins at hand are compatible with the methods available [3]. Moreover, structures of protein complexes are often extremely difficult to determine by experiments, even without the involvement of a membrane. Thus, when a protein complex structure has not yet been experimentally determined, computational tools can be used to construct atomic models [4]. A protein docking program can take component proteins, called subunits, as input and assemble them into models of the protein complex. Many general protein docking methods and specialized versions thereof have been publicly released, such as ZDOCK [5], HADDOCK [6], ClusPro [7], RosettaDock [8], HEX [9], SwarmDock [10], and ATTRACT [11]. Even protein structure prediction methods like AlphaFold [12] have been tweaked to be able to output multimeric structures [13]. The rigid-body docking method LZerD [14-17] in particular has been consistently ranked highly in the server category in CAPRI [18, 19], the blind communitywide assessment of protein docking methods.

The fact that proteins in vivo are not generally interacting in isolation in a uniform environment is often confounding to computational modeling of complexes. Even with state-of-the-art modeling techniques, existing docking methods struggle to rigorously handle environments other than a uniform aqueous environment [20, 21]. Membranes create an environment where hydrophobic surfaces are not strongly energetically incentivized to be buried in the protein-protein interface. For example, in the transmembrane halorhodopsin protein family as found in halobacteria, which is included in the benchmark of Mem-LZerD, the protein-protein interface is not especially rich in hydrophobic amino acids relative to the remainder of the molecular surface, much of which participates in the protein-lipid interface [22]. Highlighting the utility of docking methods, a halorhodopsin structure for *Halobacterium salinarium* was available in 2000, but no

structure for *Natronomonas pharaonic* was available until 2009 [23]. Homology-based methods can be used to model the subunits, and a docking method can then be used to explore the space of interaction poses. Other proteins do not wholly embed in the membrane, but instead pass only partway through or interact only with the membrane surface. These peripheral membrane proteins are likewise important and are implicated for example in sensitivity to membrane composition [24].These broad categories of membrane protein break down further into classes with substantial mechanistic differences, from the purely α-helical transmembrane regions most commonly considered by computational methods, transmembrane β-barrels, to peripheral membrane proteins attaching to the membrane with amphipathic helices [25] or with hydrophobic loops [26]. Transience in certain interactions between these proteins can render them difficult to directly consider in vitro [27], but more accessible via computational modeling [28]. It is then clear that techniques capable of modeling interactions involving membranes have the potential to elucidate many cellular processes in many biological contexts. Detailed mechanistic understanding of membrane protein complexes currently represents a major knowledge gap in molecular biology and is the subject of much active investigation [29]. Recent studies have shown that protein structure prediction methods can enable combinatorial modeling of putative interactions among, for example, the cytochrome c maturation system I proteins of *E. coli* [28].

Several computational techniques have been developed which predict the modes of interaction of proteins in a membrane environment. MPDock, part of the RosettaMP software collection, takes a specification of membrane chemistry and dimensions to model the assembly of transmembrane complexes from bound experimental structures [30]. The bound subunits were pulled apart, repacked according to the algorithm of Rosetta, and then pulled back together. Memdock carries out rigid-body docking of α-helical membrane proteins by constraining their orientation, before a finer-grained refinement procedure, and makes the assumption that the whole-input center of mass roughly coincides with the membrane midplane [31, 32]. JabberDock for membrane proteins represents the subunits with a volume map incorporating dynamics information from an expensive 70ns molecular dynamics simulation and uses particle swarm optimization techniques to explore the pose space, which required strict constraints on the pose space [33]. In summary, MPDock requires bound native structures as input and requires manual processing, Memdock was only tested on α-helical proteins and requires assumptions about the membrane location, and is further

unable to include soluble regions of proteins in the modeling, and JabberDock requires substantial molecular dynamics calculations and is limited to exploring a tight region of the search space the precludes tolerance for misorientation. These existing analyses require orientations taken from bound complex structures, rather than orientations predicted separately for each subunit. In the context of blind modeling, however, the precise orientations which individual subunits take on upon binding are not known. A method for blind membrane docking should predict the membrane orientations of the input subunits and have a docking search space which is narrow enough to exclude prediction errors, but broad enough to tolerate reasonable errors in orientation predictions.

Mem-LZerD, which we developed in this work, is based on the LZerD rigid-body docking method and its extensions [14-17, 34-36] LZerD uses a soft surface representation of the protein subunits based on geometric hashing [37] and 3D Zernike descriptors (3DZDs) [38-43], which allows for fast generation of docking poses without considering side-chain repacking. The geometric hashing procedure originally used internally by regular LZerD also admits more site-specific orientation and translation restrictions. Mem-LZerD targets any transmembrane protein complexes, as well as peripheral membrane proteins. The geometric hashing data structure used by Mem-LZerD is newly augmented with the positioning of each sample point relative to the membrane generated by the Positioning of Proteins in Membranes (PPM) algorithm [44, 45] , as well as the angular orientation in the same membrane. Pruning the search space in this way, skipping infeasible poses, yielded a running time 74 times faster on average compared to regular LZerD without search space or model constraints. This speedup highlights that for membrane proteins, most of the calculation time in regular LZerD is wasted on infeasible poses, e.g. those which are sideways or entirely outside the membrane, which then contaminates the output model ranking. We will directly show that the examined regime is inaccessible to ordinary rigid-body docking and that interactions of both transmembrane and peripheral membrane proteins are accessible in this framework. Mem-LZerD yielded acceptable models within the top 10 models for 13 of 21 (61.9%) unbound docking targets of the Memdock benchmark set, according to the CAPRI criteria, while Memdock was able to model only 4 (19%) targets, or 36.4% of the 11 targets for which the protocol modeled unbound subunit structures at all. On that smaller set, Memdock successfully modeled 5 (45.5%) of the targets. On our separate transmembrane protein benchmark set, Mem-LZerD successfully modeled 35 of the 44 (79.5%) unbound benchmark docking

targets, while on a peripheral membrane protein benchmark set, Mem-LZerD successfully modeled 54 of 92 (58.7%). Mem-LZerD has been incorporated into the LZerD webserver, available at https://lzerd.kiharalab.org. We further show that the protocol pipeline of OPM/PPM [44], Mem-LZerD, and CHARMM-GUI [46] can produce ready-for-simulation files of sampled binding poses in explicit lipid membranes.

RESULTS AND DISCUSSION

Overview of Mem-LZerD

The docking procedure of Mem-LZerD follows the observation that presence of a lipid membrane restricts the poses two proteins may take on when they assemble into a complex. Mem-LZerD builds assembled complex models by independently orienting input proteins using PPM [44], then applying a geometric hashing-based procedure adapted from LZerD with augmentations that allow pruning the search space to sample membrane-bound poses, before a final clustering and scoring procedure yield the final outputs The overall procedure of Mem-LZerD is diagrammed in Figure 1a.

The first step is to orient both the receptor and ligand protein subunits separately in the membrane using PPM, which minimizes its computed free energy of transfer between the aqueous and membrane environments. PPM has been tested on thousands of membrane proteins and validated against hundreds of experimental results [44]. PPM, however, does not in general generate precisely the orientations the subunits take on in their bound states, but the search and sampling procedure of Mem-LZerD is sufficiently tolerant that such precision is not necessary. Transmembrane proteins are immersed in the membrane and therefore more clearly restrained by it, while peripheral membrane proteins merely interact with the membrane surface and are less clearly restrained.

In the next stage, Mem-LZerD searches the pose space using the LZerD algorithm while accounting for the restricted pose space using an augmented data structure. Unlike the data structures used in original LZerD, the newly augmented geometric hashing in Mem-LZerD facilitates restricting the search space without the expense of running the full pipeline and post-filtering the output. The two subunits are assumed to be oriented to the same membrane. The residuals of the protein surface sample point height, a novel

development, and the angles between the transformed membrane planes, as illustrated in Figure 1b, established in the literature and validated in this work, together then constrain the pose space. These simple criteria facilitate efficient search of the pose space without wasting time calculating intermediate scores for infeasible poses. The cutoffs for unbound docking for a differently formulated height constraint and the tilt constraint have been suggested in the literature as 8 Å and 0.4 radians respectively. For the constraints as newly formulated in Mem-LZerD, we propose the same cutoffs. We calculated the enrichment factor (EF) and recall where applicable across the training set targets between the baseline LZerD sampling and the sampling with constraints applied. As shown in Figure 2c, that same setting exhibits the highest EF value before a dramatic loss of recall is observed. Supplemental Video S1 illustrates the difference between this procedure and the original LZerD search using the chosen constraint cutoffs of 8 Å and 0.4 radians.

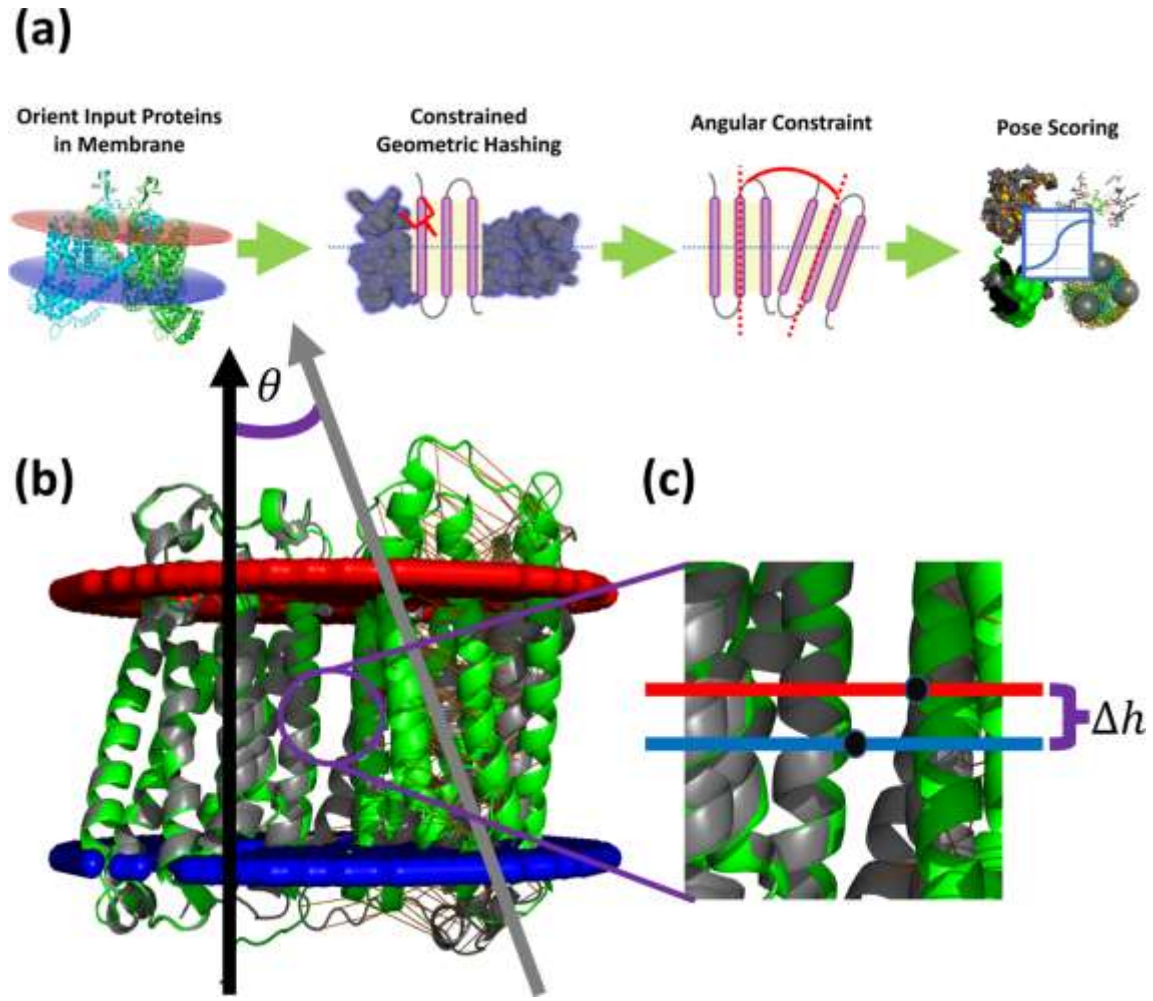

Figure 1. (a) Overall flow of the Mem-LZerD method. **(b)** Tilt constraint used by Mem-LZerD. The black and grey arrows represent example the axes perpendicular to the membrane planes as oriented by PPM, while θ is the tilt angle between those axes. The red and blue boundaries represent the inner and outer membrane surfaces predicted by PPM for the receptor subunit. **(c)** The height constraint used by Mem-LZerD. The black dots represent points on the molecular surface sampled by the initial stages of LZerD, while the difference between the pre-docking oriented heights relative to the membrane Δh is the height used to prune the docking search.

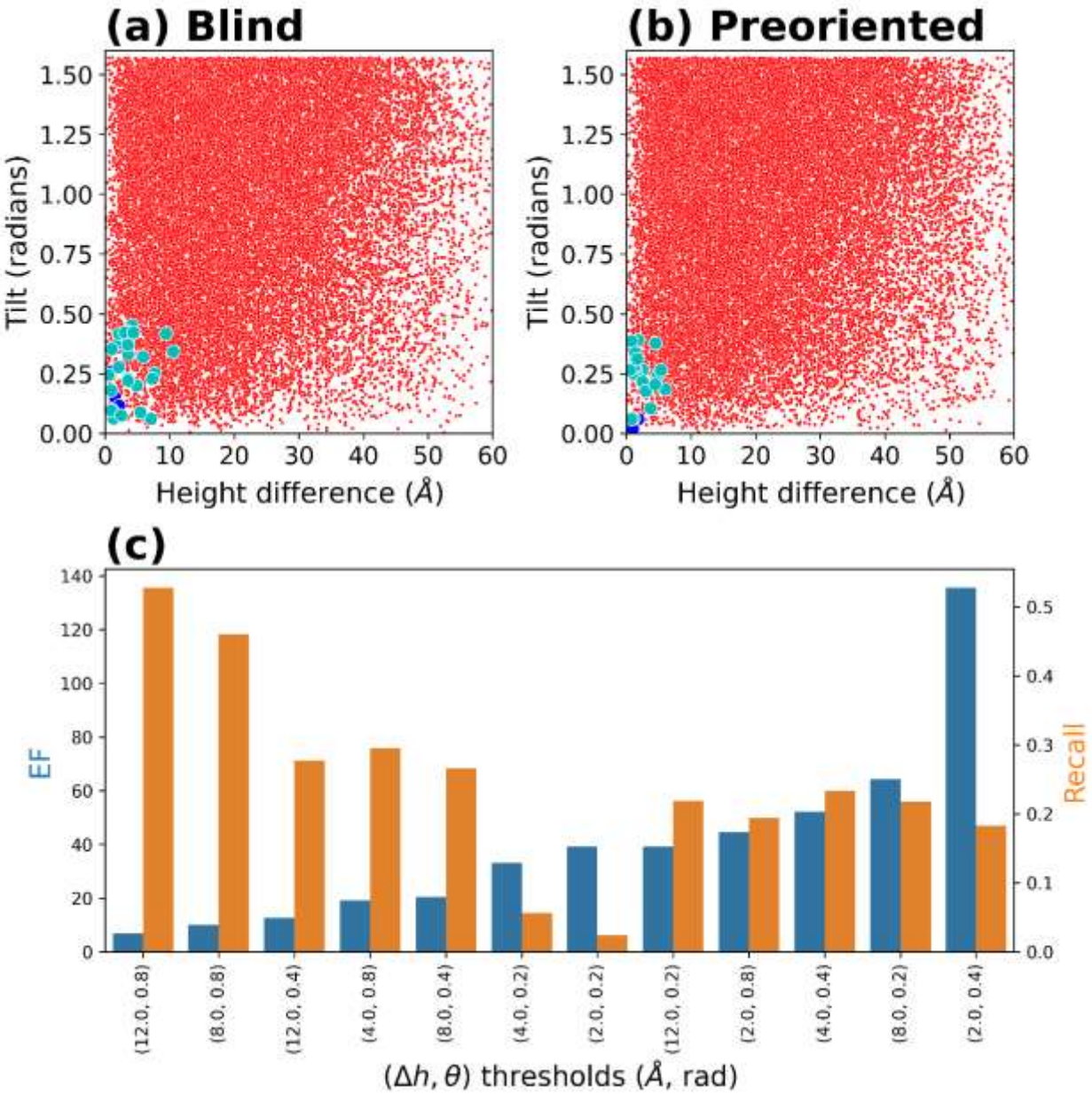

Figure 2. Deviation from ideal membrane spatial positioning and orientation using (a) blindly oriented and (b) preoriented docking inputs for PDB 1M56, as included in the usual top 50,000 models from LZerD. Red: incorrect quality models. Cyan: acceptable quality models. Blue: medium models. Green: high quality models. Even when blindly predicted inputs are used, 0.4 radians tilt and 8 Å height difference are sufficient to capture most models of acceptable or better quality. (c) Validation of the 0.4 radians tilt and 8 Å height difference cutoffs. Blue: enrichment factor of the constrained pose space. Orange: recall of the constrained

pose space. When parameter combinations are sorted by enrichment factor, recall sharply declines after 0.4 radians tilt and 8 Å height difference.

Overall docking results

Mem-LZerD was trained and benchmarked on nonredundant sets of transmembrane proteins, as described in Methods, and was additionally benchmarked on a nonredundant set of monotopic membrane proteins. The main evaluation results are summarized in Table 1 and Table 2, covering the existing benchmark set [32] and our new benchmark set respectively.

To examine the precision of docking using Mem-LZerD versus past rigid-body methods, we compared the performance of Mem-LZerD against the Memdock benchmark set [32]. The Memdock algorithm is designed specifically for α-helical transmembrane proteins, rather than general membrane proteins which may be β-barrels or not transmembrane at all. Thus, we compare using Memdock's original benchmark set of 21 α-helical transmembrane complexes. Considering top-10 performance on its benchmark set, Memdock achieved a success rate of 71.4% for bound docking, while Mem-LZerD achieved a success rate of 76.2%. On this same benchmark, the baseline LZerD pipeline succeeded on no targets for unbound docking and 2 of 21 (9.5%) targets for bound docking. Transmembrane docking targets were thus shown to largely require specialized methods, and Mem-LZerD achieved a higher success rate than such existing specialized methods.

For unbound docking on the Memdock benchmark, results from past docking experiments using both Memdock and JabberDock were available, and we evaluated the unbound docking performance of Mem-LZerD against these. Here, Mem-LZerD achieved an overall success rate of 61.9%, while Memdock and JabberDock achieved 19.0% and 33.3% respectively overall. However, Memdock skipped targets where obvious templates were unavailable, and thus 10 targets were counted as yielding 0 hits for both sets of previous results. When retabulating the success rates on only the 11 targets where Memdock included unbound docking, Mem-LZerD achieved a success rate of 54.6%, while Memdock and JabberDock achieved 36.4% and 63.6% respectively. While this appears to suggest that Mem-LZerD does

not overcome the state-of-the-art performance of JabberDock, we note that the original experiments for Memdock and JabberDock did not include blind predictions of the membrane orientations of the input subunits, but rather took the orientations directly from complex structures in the OPM database. The 54.6% success rate of unbound docking using Mem-LZerD is thus while blind to the ground truth orientation, while the other methods assumed the ground truth orientation as their starting points. To compare unbound docking performance more fairly, we additionally calculated preoriented unbound input models by superimposing them individually to their native structures as oriented in OPM. The success rate was then 66.7% overall, and 63.6% on the 11 unbound Memdock targets. Mem-LZerD thus performed equivalently to JabberDock on preoriented inputs, despite requiring no expensive molecular dynamics simulation, while still performing well on targets with only predicted orientations.

On the additional transmembrane benchmark unbound test set, which included both α-helical and non-α-helical transmembrane proteins such as beta barrels, 35 of 44 targets (79.5%) were modeled to at least acceptable CAPRI quality. On the peripheral benchmark unbound test set, just 15 of 92 targets (16.3%) were modeled to at least acceptable CAPRI quality. This success rate is substantially lower than what was observed for transmembrane docking, as might be expected from the intuition that peripheral membrane proteins should be more difficult to orient to the membrane, especially when the subunits are oriented individually. Indeed, an unconstrained docking search sampled poses of at least acceptable CAPRI quality for 74 of 92 targets (80.4%). It should also be noted that, as shown in Supplementary Table S1, the standard LZerD pipeline was able to rank poses of at least acceptable CAPRI quality in the top 10 for 52 of 92 targets (56.5%), demonstrating that methods designed for soluble proteins are better at selecting good peripheral complex poses than the state-of-the-art PPM is at orienting the subunits. Since peripheral membrane proteins are by definition not immersed in the membrane, they are physically closer to soluble proteins than transmembrane proteins. This disparity confirmed that most of the peripheral targets are not sufficiently well oriented by PPM to dock using this method of constraining the search space. As shown in Figure 5abc, the Mem-LZerD decoy set for unbound peripheral membrane complex docking has a substantially worse distribution of all CAPRI measures as compared to transmembrane docking results. In addition to the sampling constraints, the calculation of the membrane transfer energy for the scoring function is also dependent on the input orientation. To investigate what effect improvements to the subunit

orientation predictions could have on the accuracy of the docking predictions, we recomputed the peripheral membrane protein targets using their bound orientations by superimposing the unbound subunits into the native structure taken from the OPM database, in the same way as in the transmembrane comparison. By doping the pipeline with these bound orientations, the performance jumped to 54 of 92 targets (59.3%) modeled to at least acceptable CAPRI quality, demonstrating that despite the mostly-soluble nature of peripheral membrane proteins, accurate orientation information can still improve docking outcomes. As additionally shown in Figure 5d, the substitution of ground truth orientations for the poor orientations of PPM dramatically improves the interface accuracy, measured by I-RMSD, of most targets. Thus, future expansions of PPM or the inclusion of additional information from experiment have the potential to change the outcome of peripheral complex docking from likely unsuccessful to likely successful.

Target	Bound				Unbound Blind			Unbound Preoriented [a]			
	Mem-LZerD I-RMSD	Mem-LZerD RFH	Memdock RFH	LZerD RFH	Mem-LZerD I-RMSD (Å)	Mem-LZerD RFH	LZerD RFH	Mem-LZerD I-RMSD (Å)	Mem-LZerD RFH	Memdock RFH	JabberDock RFH
1e12_A_C	0.6	6	(28)	(268)	10.2	(80)	(97)	3.5	10	(57)	2
1m0l_A_C	2.2	1	(74)	(1429)	11.4	(28)	(709)	4.9	(17)	(49)	7
1m56_A_C	1.1	1	2	(97)	1.2	1	(17)	2	2	(11)	X
1q90_B_S	2.3	2	1	(2661)	2.7	1	(1106)	1.9	1	1	5
1rc2_A_B	1.2	2	2	(74)	0.8	1	(61)	0.9	1	n/a	n/a
1rwt_A_C	12.8	(56)	(25)	(19150)	5.8	(1181)	(19985)	19.2	(775)	n/a	n/a
1u7g_A_C	0.6	2	2	2	1.1	2	(38)	1.3	2	n/a	n/a
1zoy_C_D	3.5	1	1	(155)	3.8	10	(615)	3	1	1	(159)
2a65_A_B	5.6	(24)	4	9	4.4	5	(331)	10.8	(11)	n/a	n/a
2f2b_A_C	3.1	1	1	(145)	3.1	1	(49)	3.2	2	n/a	n/a
2qjy_A_D	0.7	2	X	(1749)	1.1	2	(2821)	4.3	4	1	3
3chx_B_J	11.7	(6745)	X	(1005)	14.8	X	X	17.2	X	X	8
3dh4_A_B	1.6	7	3	(557)	4.6	(13)	(318)	2.1	5	n/a	n/a
3h5m_A_B	0.7	1	1	(114)	3.8	1	(375)	3.7	1	n/a	n/a
3hfx_A_B	14	(382)	6	(13054)	17.3	(969)	(11843)	19.3	(236)	n/a	n/a
3kly_A_B	0.4	1	1	(165)	1.9	1	(366)	2	4	1	5
3m73_A_K	0.8	1	1	(2635)	0.8	4	(2651)	0.9	1	n/a	n/a

3oe0_A_B	10.8	(119)	X	(2222)	17.3	X	X	13.5	X	(45)	X
3rvy_A_B	1.3	1	5	(226)	2	4	(129)	2.1	1	X	X
3tui_A_B	1	1	1	(233)	1.7	1	(365)	1.6	1	n/a	n/a
4dkl_A_B	2.2	1	4	(395)	16.4	X	X	18.1	X	X	1
Total Successes:		**16 (76.2%)**	**15 (71.4%)**	**2 (9.5%)**		**13 (61.9%) (54.6% excl. n/a)**	**0 0.0%**		**14 (66.7%) (63.6% excl. n/a)**	**4 (19.0%) (36.4% excl. n/a)**	**7 (33.3%) (63.6% excl. n/a)**

Table 1. Docking performance of the 21 individual targets of the Memdock benchmark set. RFH is the rank of the first CAPRI-acceptable model generated, if any, for a given target. RFH must exist and be at most 10 for modeling to be considered successful. n/a indicates that there was no unbound model for a target at the time of the study. X indicates that there no docked models of at least acceptable quality in the analyzed output; for Mem-LZerD, this is limited to 50,000, the pre-clustering model cutoff; for Memdock, this is limited to the top 100 models. We considered only the top 10 models from either method in our evaluation, but scored model ranks worse than 10 are shown here for completeness in parentheses. The I-RMSD columns list the best I-RMSD among the top 10 models. Separate preoriented docking outcomes are not show for regular LZerD runs since the original LZerD pipeline does not consider input model orientation. [a] These evaluations of Memdock and JabberDock from the paper first describing their use for membrane docking used premade orientations from OPM, which are orientations of the full bound complexes rather than the subunits independently. The Mem-LZerD unbound benchmark otherwise shown is fully unbound docking, with membrane orientations calculated by PPM separately for each subunit without regard to the full complex. However, here we additionally show Mem-LZerD results when using ground truth orientations as in the original Memdock and JabberDock studies.

	Bound			Unbound			Regular LZerD Unbound		
Target	**I-RMSD (Å)**	**L-RMSD (Å)**	f_{nat}	**I-RMSD (Å)**	**L-RMSD (Å)**	f_{nat}	**I-RMSD (Å)**	**L-RMSD (Å)**	f_{nat}
1a0s	1.0	2.3	0.78	(16.9)	(27.8)	0.00	(36.69)	(68.60)	(0.00)
1kqf	1.6	2.7	0.46	2.5	5.1	0.22	(16.29)	(33.42)	(0.00)
1p7b	1.3	2.9	0.62	4.6	8.1	0.12	(17.28)	(32.12)	(0.02)
2yvx	(23.1)	(38.9)	(0.00)	1.5	2.5	0.52	(28.46)	(60.53)	(0.00)
3a7k	1.4	3.2	0.51	2.0	3.6	0.54	(22.47)	(33.77)	(0.00)
3b4r	1.7	2.7	0.53	2.3	5.4	0.49	(16.74)	(33.69)	(0.00)
3b8n	(22.3)	(44.1)	(0.00)	(48.9)	(59.8)	0.00	(47.60)	(51.36)	(0.00)
3pjz	2.0	4.8	0.44	2.2	3.6	0.46	(16.98)	(35.79)	(0.00)
3qnq	1.6	3.7	0.42	1.3	2.6	0.63	1.29	2.57	0.63
3ux4	1.4	3.3	0.63	2.3	5.1	0.51	(14.75)	(28.60)	(0.00)
4ezc	1.8	3.7	0.39	1.4	2.0	0.64	(15.83)	(32.30)	(0.00)
4hkr	1.7	3.1	0.39	(11.2)	(12.2)	(0.10)	(17.99)	(28.63)	(0.00)
4hyg	2.8	5.6	0.46	5.0	6.5	0.51	(24.17)	(58.72)	(0.00)
4o6m	0.6	1.9	0.85	1.1	2.6	0.70	1.06	3.76	0.70
4p6v	0.9	2.0	0.84	2.5	3.8	0.64	(20.67)	(43.74)	(0.00)
4pl0	(16.9)	(32.6)	(0.00)	(21.8)	(36.3)	(0.00)	(30.87)	(57.20)	(0.00)
4r1i	0.7	1.3	0.80	1.2	2.6	0.78	1.17	2.59	0.78
4ri2	2.5	4.8	0.40	4.8	6.4	0.26	(13.04)	(23.82)	(0.03)
4rp8	2.1	4.1	0.58	2.2	4.0	0.55	(23.41)	(56.31)	(0.00)
4wd8	4.2	8.9	0.24	4.6	9.0	0.18	1.96	3.88	0.51
5a1s	0.8	1.4	0.83	2.3	4.5	0.79	2.32	4.54	0.79
5aex	0.5	1.1	0.94	(13.2)	(21.5)	(0.02)	(36.06)	(68.22)	(0.00)
5i6c	1.9	5.8	0.33	2.9	3.9	0.44	(21.19)	(56.41)	(0.00)
5j4i	0.8	1.8	0.75	3.4	4.7	0.48	(21.82)	(61.91)	(0.00)
5o65	0.9	1.9	0.91	1.9	3.4	0.44	(22.93)	(40.19)	(0.00)
5sv9	2.2	4.2	0.44	4.7	6.8	0.23	(23.02)	(42.10)	(0.00)

6c96	(4.6)	(12.2)	(0.16)	(6.9)	(11.6)	(0.02)	(38.81)	(93.12)	(0.00)
6hcp	2.1	6.7	0.48	(40.9)	(43.2)	(0.00)	(39.88)	(70.88)	(0.00)
6k1h	2.9	5.9	0.36	2.0	2.7	0.43	(28.77)	(61.40)	(0.00)
6l85	0.9	2.7	0.90	3.2	4.0	0.43	(7.84)	(13.92)	(0.01)
6n1g	0.6	1.4	0.84	2.7	6.1	0.38	(20.73)	(49.61)	(0.00)
6o58	(20.8)	(67.3)	(0.00)	(23.2)	(46.6)	(0.00)	(24.87)	(53.92)	(0.00)
6rko	0.8	1.8	0.72	4.8	8.3	0.49	(4.77)	(10.08)	(0.49)
6rvx	2.1	6.0	0.45	3.8	7.3	0.22	(33.71)	(60.68)	(0.00)
6vgc	2.8	5.6	0.28	3.6	12.8	0.41	(21.14)	(33.60)	(0.00)
6xjh	1.3	1.9	0.59	3.8	6.0	0.22	(17.85)	(34.48)	(0.00)
6y7f	1.3	5.7	0.63	3.3	14.0	0.38	(13.83)	(49.53)	(0.00)
6ys8	(9.1)	(20.0)	(0.01)	(14.7)	(24.5)	(0.00)	(15.03)	(30.88)	(0.00)
7ck6	2.9	9.6	0.24	1.9	6.0	0.37	(16.94)	(40.07)	(0.00)
7cxr	2.6	5.9	0.45	2.8	5.1	0.52	2.82	5.11	0.31
7czb	2.0	6.4	0.68	3.3	7.4	0.56	(27.62)	(58.81)	(0.00)
7jk8	1.8	3.7	0.69	3.5	5.1	0.28	(16.30)	(32.98)	(0.00)
7lhv	1.0	2.4	0.67	5.3	9.8	0.35	(33.22)	(72.68)	(0.00)
7oqz	1.5	3.2	0.38	2.4	3.9	0.40	(13.53)	(23.66)	(0.05)

Table 2. Docking performance of the 44 individual targets of the Flex-LZerD benchmark test set. Parentheses indicate that no models of at least CAPRI-acceptable quality were ranked within the top 10. The columns list the best of each measure among the top 10 models.

Case Study 1: Zinc metalloprotease mjS2P (PDB 3B4R)

Highlighted in Figure 3a is the zinc metalloprotease mjS2P complex from *Methanocaldococcus jannaschii*, a protease capable of cleaving proteins in the lipid membrane environment [47]. This complex is a key part of signaling by regulated intramembrane proteolysis, a signaling mechanism which has been established as conserved from bacteria to humans [48]. Understanding the mechanisms of mjS2P can thus be used to elucidate human intramembrane proteases. Although the mechanism of this enzyme is conserved and bacterial homologs were known even in 2007 when its PDB entry 3B4R was deposited, even modern template search techniques such as HHpred [49], using database PDB_mmCIF70_17_Apr, found hits for only a small region of the protein. While this target was not tested in the Memdock or JabberDock studies, a run of AlphaFold as a substitute failed to model this complex, generating a model of incorrect CAPRI quality with an I-RMSD of 19.1 Å, and L-RMSD of 43.2 Å, and an f_{nat} of 0.01, shown in the right of Figure 3a. Although this model looks passably folded, it does not appear to even contain an appropriate transmembrane axis. Mem-LZerD on the other hand was able to generate a model of acceptable CAPRI quality with an I-RMSD of 2.3 Å, and L-RMSD of 5.4 Å, and an f_{nat} of 0.49, shown in the left of Figure 3a. The inclusion by Mem-LZerD of reversed orientations was key to the successful modeling of this target, as otherwise Mem-LZerD would have only yielded incorrect models.

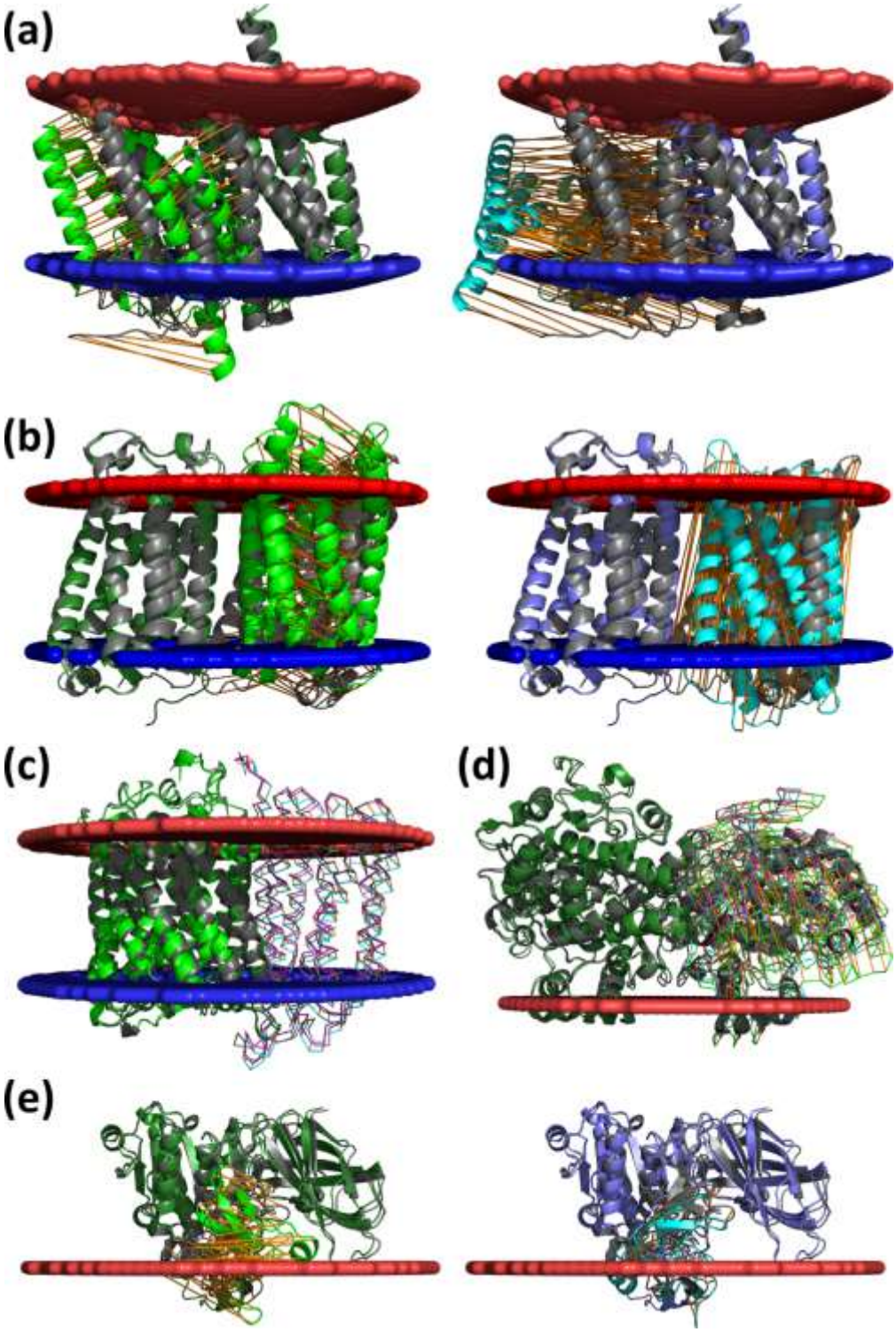

Figure 3. Example modeling of membrane protein complexes. Gray: the native structure. Red and blue: the membrane locations calculated by PPM. Orange: Cα deviations of one subunit when the other is

superimposed. **(a)** Zinc metalloprotease mjS2P (PDB 3B4R). Left: Mem-LZerD yielded a model (green/dark green) with an I-RMSD of 2.3 Å, and L-RMSD of 5.4 Å, and an f_{nat} of 0.49. Right: AlphaFold yielded a model (cyan/slate) with an I-RMSD of 19.1 Å, and L-RMSD of 43.2 Å, and an f_{nat} of 0.01. **(b)** Elongation of very long chain fatty acids protein 7 (PDB 6Y7F). Left: Mem-LZerD yielded a model (green/dark green) with an I-RMSD of 3.3 Å, and L-RMSD of 14.0 Å, and an f_{nat} of 0.38. Right: AlphaFold yielded a model (cyan/slate) with an I-RMSD of 20.2 Å, and L-RMSD of 35.0 Å, and an f_{nat} of 0.00. **(c)** Poses of medium CAPRI quality generated by Mem-LZerD for cytochrome-c oxidase (PDB 1M56). Green: the unbound receptor subunit. Cyan: first hit, an I-RMSD of 1.5 Å, and L-RMSD of 2.4 Å, and an f_{nat} of 0.71. Magenta: second hit, with an I-RMSD of 1.2 Å, and L-RMSD of 1.9 Å, and an f_{nat} of 0.84. Orange: displacements between the two poses, with an RMSD of 2.5 Å RMSD and maximum of 3.6 Å. **(d)** Prostaglandin G/H synthase 2 (PDB 1CX2). Mem-LZerD yielded a model of acceptable CAPRI quality (green) with an I-RMSD of 3.2 Å, and L-RMSD of 6.4 Å, and an f_{nat} of 0.26, while doping with ground truth subunit orientations yielded a model of medium CAPRI quality (cyan) with an I-RMSD of 1.7 Å, an L-RMSD of 2.7 Å, and an f_{nat} of 0.51. Blind and doped model displacements are shown in orange and magenta respectively. **(e)** Pancreatic triacylglycerol lipase/colipase complex (PDB 1LPA). Left: Mem-LZerD yielded an incorrect model with an I-RMSD of 10.7 Å, and L-RMSD of 18.4 Å, and an f_{nat} of 0.02. Right: Mem-LZerD doped with ground truth subunit orientations yielded a model of acceptable CAPRI quality (cyan) with an I-RMSD of 3.7 Å, an L-RMSD of 5.0 Å, and an f_{nat} of 0.54.

Case study 2: Elongation of very long chain fatty acids protein 7 (PDB 6Y7F)

Highlighted in Figure 3b is the human ELOVL7 elongase complex, which is responsible for catalyzing the fatty acid elongation cycle [50]. Elongases have been demonstrated to cause a variety of serious genetic diseases in humans [51-53]. In the ELOVL7 homodimer observed by experiment, the substrate binds deep in a narrow tunnel formed by the structure of one subunit. The substrate binding site is not directly formed by the protein-protein interaction interface. The active site and interaction surface of this enzyme were noted to not be well-conserved in 2020 when its PDB entry 6Y7F was deposited, and modern template search techniques such as HHpred [49], using database PDB_mmCIF70_17_Apr, found no hits other than

PDB 6Y7F itself. While this target was not tested in the Memdock or JabberDock studies, a run of AlphaFold as a substitute failed to model this complex, generating a model of incorrect CAPRI quality with an I-RMSD of 20.2 Å, and L-RMSD of 35.0 Å, and an f_{nat} of 0.00, shown in the right of Figure 3b. AlphaFold relies on coevolutionary signals extracted from sequence databases, but the protein-protein interface in this target is not well-conserved. While the experimentalists observed the complex in a head-to-tail dimer both in crystal and in solution, AlphaFold instead generated head-to-head dimer models. Mem-LZerD on the other hand was able to generate a model of acceptable CAPRI quality with an I-RMSD of 3.3 Å, and L-RMSD of 14.0 Å, and an f_{nat} of 0.38, shown in the left of Figure 3b. The inclusion by Mem-LZerD of reversed orientations was key to the successful modeling of this target as well, as otherwise Mem-LZerD would have only yielded incorrect models.

Case study 3: Cytochrome-c oxidase (PDB 1M56)

Highlighted in Figure 3c is a cytochrome-c oxidase complex from *Cereibacter sphaeroides*, a transmembrane enzyme found in the inner mitochondrial and cell membranes of bacteria [54]. Cytochrome-c oxidase is critical to the respiration of bacteria and generates a proton gradient across the membrane. For this target, both Memdock and JabberDock failed to retrieve a model of acceptable CAPRI quality in unbound docking, yielding only models of incorrect CAPRI quality within the top 10 models. Mem-LZerD on the other hand was able to generate a two models of medium CAPRI quality, one with an I-RMSD of 1.5 Å, and L-RMSD of 2.4 Å, and an f_{nat} of 0.71, and another with an I-RMSD of 1.2 Å, and L-RMSD of 1.9 Å, and an f_{nat} of 0.84. These two models both exceeded the criteria for acceptability, but as shown in Figure 3c are globally different poses with an overall displacement of 2.5 Å RMSD and individual Cα displacements as high as 3.6 Å. Mem-LZerD poses such as these can, for example, be used to instantiate molecular dynamics simulations with distinct but reasonable initial conditions. Figure 2ab demonstrates the utility of reducing the search space in terms of height and tilt. In essence, the better the membrane orientation predictions, the tighter the distribution of models of at least acceptable CAPRI quality in the search space. After feasible poses have been generated, they are clustered and scored using a combined scoring function that accounts for both the protein-protein interface and the immersion of the proteins in the membrane.

Case study 4: Prostaglandin G/H synthase 2 (PDB 1CX2)

Highlighted in Figure 3d is a murine prostaglandin G/H synthase 2 (PTGS2) complex, a peripheral membrane enzyme found in the nuclear and endoplasmic reticulum membranes of mice [55]. PTGS2 is involved in inflammatory response pathways, and interactions with homologous human proteins are the molecular basis of many non-steroidal anti-inflammatory drugs (NSAIDs) [56, 57]. PTGS2 binds to membranes peripherally via a helical amphipathic domain [58], which the protein-protein interface of PTGS2 does not include [59]. For this target, Mem-LZerD using inputs blindly oriented by PPM was able to produce a model of acceptable CAPRI quality with an I-RMSD of 3.2 Å, and L-RMSD of 6.4 Å, and an f_{nat} of 0.26. While this target was one of the few peripheral membrane complex targets where the blind orientation prediction was sufficient to achieve acceptable structure modeling, it can in fact still benefit from the integration of orientation information. When instead modeling using the full-complex orientation from OPM, Mem-LZerD yielded a model of medium CAPRI quality with an I-RMSD of 1.7 Å, an L-RMSD of 2.7 Å, and an f_{nat} of 0.51.

Case study 5: Pancreatic triacylglycerol lipase with colipase (PDB 1LPA)

Highlighted in Figure 3e is a human pancreatic triacylglycerol lipase (PTL), a peripheral membrane protein involved in the metabolism of fats [60, 61], complexed with a porcine colipase (CLPS), a cofactor which facilitates membrane anchoring [62]. PTL is understood to break down long-chain fatty acids and acts preferentially on insoluble substrates [60, 61]. Due to the presence of amphipathic bile salts in the physiological environment of PTL, the smaller CLPS is required as a cofactor to facilitate a binding mode with the catalytic site of PTL in sufficiently close contact with the membrane [62]. For this target, Mem-LZerD using inputs blindly oriented by PPM was unable to produce a model of acceptable CAPRI quality, with the best of the top-10 models only reaching an I-RMSD of 10.7 Å, and L-RMSD of 18.4 Å, and an f_{nat} of 0.02, as shown in the left of Figure 3e. In fact, Mem-LZerD was unable to sample any model of acceptable CAPRI quality, indicating that blind prediction of the subunit orientations by PPM did not properly characterize the feasible region of docking poses. This incorrect modeling outcome can be attributed to the biophysical properties of PTL, which has not been observed to bind strongly to the membrane without CLPS [62]. However, regular LZerD without constraints also did not yield a model of acceptable CAPRI quality in the top-10 models, yielding an even worse an I-RMSD of 22.3 Å, an L-RMSD of 51.8 Å, and an f_{nat} of 0.00,

suggesting that the physiological environment of the intestine may be challenging to account for with the usual scoring functions. When instead modeling using the full-complex orientation from OPM, Mem-LZerD yielded a model of medium CAPRI quality with an I-RMSD of 3.7 Å, an L-RMSD of 5.0 Å, and an f_{nat} of 0.54, as shown in the right of Figure 3e. Correct binding poses are thus sampled by the docking search, but in this case required additional orientation information to be discovered by the scoring function.

Preparation of molecular dynamics with membrane docking in the LZerD webserver

Due to the limited ability of models like AlphaFold to sample many interaction poses out-of-the-box, biologists interested in modeling the dynamics of proteins in a membrane may need to arrange individual protein chains to begin modeling the states desired, or even reasonable states. This difficulty is exemplified by Case Study 2 above, where despite experimental evidence to the contrary, the AlphaFold models of ELOVL7 took on entirely opposite orientations. Mem-LZerD can assemble ELOVL7 into reasonable bound poses which can then be modeled in explicit lipid solvent and simulated. Mem-LZerD is freely accessible via the LZerD webserver for protein docking, available at https://lzerd.kiharalab.org [16, 17], which allows users without high-performance computers or without computing experience to easily model the assembly of protein complexes. Figure 4a shows the input preparation for modeling poses of ELOVL7 using the LZerD webserver. Input files for docking can be taken directly from the OPM website https://opm.phar.umich.edu/) [44] or can be oriented using the PPM website or locally-installed application. The webserver allows users to specify residue-based distance constraints on the docking, and more information on this and all functionality can be found in previous works [16, 17] and the About pages on the webserver. However, in this case the default options are sufficient, and we can proceed to submit the docking. Shown in Figure 4b is the results page of this docking. Note that the ligand pose centroids, shown as spheres, highlight the focus of the membrane docking search. From here, we can download our desired models and upload them to CHARMM-GUI (https://www.charmm-gui.org) [46]. Figure 4c highlights the steps of processing a docked model using CHARMM-GUI. In this instance, we selected PLPC lipids and the NAMD output format. Figure 4d shows ELOVL7 solvated in the periodic membrane, and Supplementary Video S2 shows the equilibration and a 1ns production molecular dynamics trajectory of this system. With these together, we see that the dynamics simulation proceeds smoothly.

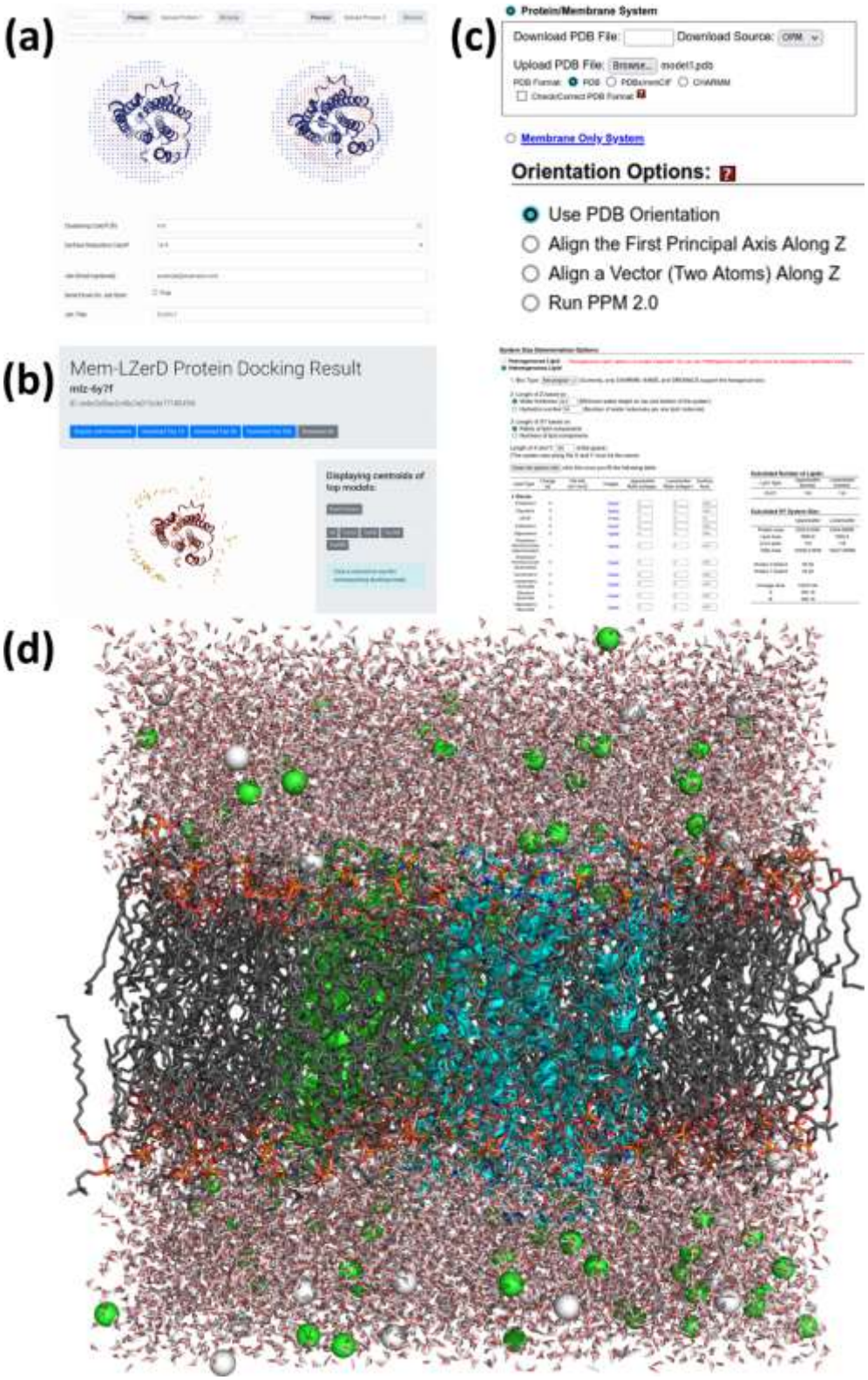
(a)
(c)
Protein/Membrane System
Download PDB File:
Download Source:
OPM
Upload PDB File:
Browse...
model1.pdb
PDB Format:
PDB
PDBx/mmCIF
CHARMM
Check/Correct PDB Format:
Membrane Only System
Orientation Options:
Use PDB Orientation
Align the First Principal Axis Along Z
Align a Vector (Two Atoms) Along Z
Run PPM 2.0
(b)
Mem-LZerD Protein Docking Result
mlz-6y7f
Displaying centroids of top models:
(d)

Figure 4. Example workflow using the LZerD webserver to prepare and run a molecular dynamics simulation of a docked model of target elongation of very long chain fatty acids protein 7 (PDB 6Y7F) in the membrane. **(a)** PPM-oriented receptor and ligand protein models uploaded to the LZerD webserver submission page. Default settings are used in the absence of residue distance information. **(b)** Mem-LZerD docking results shown in the LZerD webserver results viewer. Each sphere shows the centroid of a sampled pose. **(c)** Certain options used in generating NAMD input files using CHARMM-GUI. A PPM-oriented PDB file was uploaded, and its precomputed orientation was kept. PLPC lipids and a box size of 100 were used to construct the explicit simulation-ready files. **(d)** The final prepared coordinates for simulation.

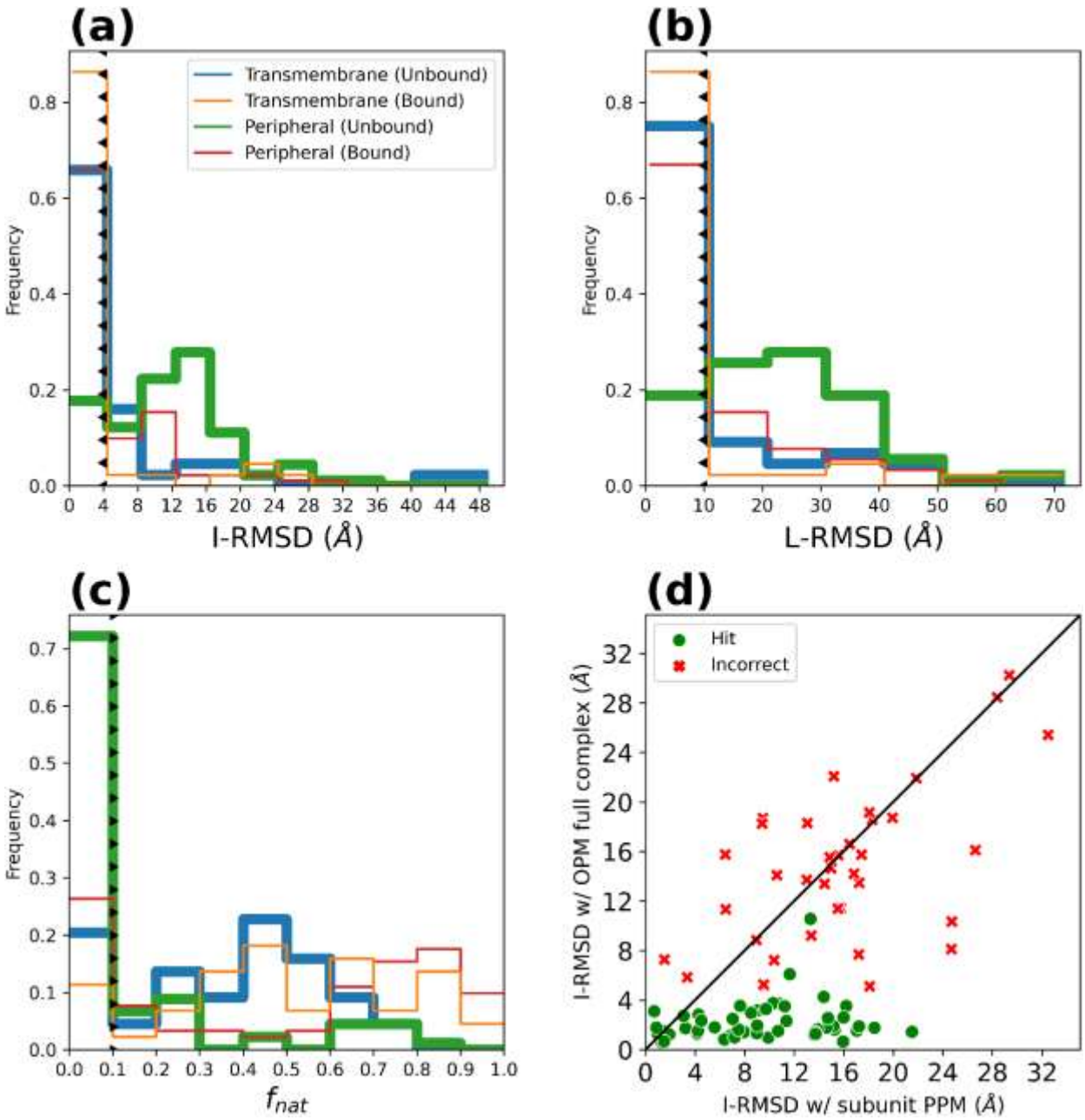

Figure 5. Docking decoy set **(a)** I-RMSD, **(b)** L-RMSD, and **(c)** f_{nat} best in top-10 distributions for transmembrane complexes vs peripheral membrane complexes. The triangle-dashed lines mark the CAPRI acceptable threshold for each metric, with the triangles pointing toward the acceptable side. **(d)** Performance of Mem-LZerD on peripheral membrane proteins using predicted versus ground truth membrane orientations. X-axis: the best I-RMSD among the top 10 models yielded by the Mem-LZerD pipeline when using the blind PPM subunit orientations. Y-axis: the best I-RMSD among the top 10 models

yielded by the Mem-LZerD pipeline when using ground truth subunit orientations by superimposing to the oriented OPM complex. Green: targets where Mem-LZerD was able to generate models of at least acceptable CAPRI quality in the top 10 when using ground truth orientations. Red: targets where Mem-LZerD failed to generate models of at least acceptable CAPRI quality in the top 10 when using ground truth orientations.

MATERIALS AND METHODS

Dataset construction

The transmembrane dataset used in this work was constructed by starting from 4218 nominally transmembrane protein structures from the OPM database [45]. Monomers were excluded, and entries were clustered at 25% sequence identity using MMseqs2 [63], yielding 390 complexes. Structure-based clustering with an MM-align [64] TM-score cutoff of 0.50 yielded 85 complexes. From these, complexes which were not oriented inside the membrane and for which the publication did not indicate that the complex was in fact studied in a membrane were excluded, or which were otherwise beyond the scope of Mem-LZerD, yielding the final transmembrane dataset of 64 complexes. 20 complexes from this dataset were separated to serve as the training set for the scoring function, while the remaining 44 complexes served as the test set. For all targets, AlphaFold v2.2.2 [12] with v2 weights and without template search was used to generate unbound subunit models.

The peripheral membrane complex dataset was constructed in a similar manner to the transmembrane dataset. Starting from 1607 complexes listed by OPM as “monotopic/peripheral”, 147 complexes with two subunits and each interacting with the membrane were extracted. After clustering as with the transmembrane dataset, 92 complexes remained, constituting the final peripheral membrane complex dataset. Peripheral complexes were not used to train the scoring function, and thus this dataset was not partitioned.

Rigid-body docking of subunits with regular LZerD

Each ligand protein structure subunit was docked with the receptor subunit using LZerD [14, 65]. LZerD is a shape complementarity-based rigid-body docking algorithm which employs a soft representation of the molecular surface to tolerate some small differences between the bound and unbound conformations. Using geometric hashing-based surface searching, LZerD generates many candidate docking poses, which are then scored according to the shape complementarity of their interfaces. For each target complex, the relevant subunit domain models were manually generated for the ligand by identifying rigid regions and removing the intervening residues. For each input domain, the set of docked models generated by LZerD was ordered by the LZerD shape score and truncated to a set of 50,000 models. Then, each set was clustered with an RMSD cutoff of 4.0 Å.

Membrane-aware pose constraints

The orientations in the membrane of models to be docked were predicted using the Positioning of Proteins in Membranes (PPM) software package [44, 45] using default settings. PPM outputs an oriented version of each input structure and also predicted the interior and exterior membrane surfaces. The separately oriented subunits were assumed to share a membrane midplane, and any differences in predicted membrane thickness were ignored. These predicted orientations are then used to augment the LZerD docking search. In LZerD, sample points on the protein surface are matched to each other in the geometric hashing discussed above. This procedure was implemented using a space-partitioning tree data structure [66], which is designed to efficiently search for points in Euclidean space by querying only relevant regions of space. By selecting appropriate planes with which to divide the space of hashed points, individual queries in the accumulation and recognition stage of the geometric hashing are made in sublinear time. In Mem-LZerD, this data structure is augmented with the distance of each point to the membrane midplane. This augmentation facilitates efficient imposition of constraints in terms of the relative midplane distance, essentially pruning the search space analyzed. For Mem-LZerD we used a relative midplane distance of 8 Å. As surface matches satisfying the relative midplane distance constraint are found, their docked orientations relative to their predicted orientations were further checked to satisfy a relative midplane axis constraint of 0.4 radians. While these are the same numerical thresholds as were previously used by Memdock, we note that they are comparable but different quantities than those constrained in Memdock.

We show a validation of these hyperparameters on the training set in Figure 2c based on the recall of models of at least acceptable CAPRI quality and the enrichment factor (EF, the ratio of the fraction of hits in the decoy set after constraining to the fraction of hits in the decoy set before constraining) of the pose space constrained to. When the parameter combinations were ordered by their corresponding EF values, we found that the recall of the constrained decoy set declined dramatically. As illustrated in Figure 2ab, nearly all of the search space outside this feasible region consists of incorrect models. Additionally, the implementation of the height constraint into the geometric hashing results in a running time 74 times faster compared to regular LZerD.

Docked model scoring

For selecting docked poses, we constructed a combined scoring function derived from methods used in the scoring of IDP-LZerD and Flex-LZerD [34-36]. This scoring function uses a bagged decision tree estimator [67] to combine the knowledge-based scoring functions GOAP [68], DFIRE [69], and ITScorePro [70], which are the three re-scoring functions combined in the usual ranksum score for competitive LZerD docking [15, 71, 72], as well as LZerD initial docking score, the cluster size from the 4 Å RMSD clustering normally used with LZerD, membrane transfer energy [73], and order statistic terms ($OS_{(1)}$, $OS_{(2)}$, and $OS_{(3)}$) highlighting the most-outlying values among the other scoring terms for each model. The LZerD shape complementarity scores and the cluster sizes are part of the regular LZerD output.

The order statics terms allow models with any outlying component scores a better chance at inclusion among the top-ranked models, even if some other component scores are low or generally disagree with each other. Each model score for all docked poses of a target is first standardized in the usual way into a Z-score. For example, the mean μ and standard deviation σ of all ITScorePro scores x_i of models of sucrose-specific porin are calculated, and the Z-score of model i will be $z_i = (x_i - \mu)/\sigma$. For scoring terms designed such that more positive values are more favorable, e.g. the LZerD shape complementarity term and cluster sizes, the values were multiplied by -1 so that lower values would uniformly be more favorable across all component scores. Thus, for all the final standardized scoring terms, a more negative Z-score is more favorable. From these, the order statistic terms were calculated for the Z-scores of the scoring terms. To compute e.g. the order statistic *OS(1)* of a model, we first check the Z-sores of all the scoring terms for

the model and select the smallest (the most favorable) Z-score. Following the same logic, *OS(2)* and *OS(3)* are the second and the third smallest Z-scores among all the Z-scores of all the scoring terms. A first-order version of this approach was previously used successfully in IDP-LZerD for disordered proteins [36], and a third-order version was used successfully in Flex-LZerD for flexible proteins [34, 35]. Here, we use the third-order version. For example, if a model has Z-scores of -1.7, -2.4, and -0.5 for the shape score, GOAP, and ITScorePro, respectively, and some arbitrary positive-valued Z-scores for the component scores, then *OS(1), OS(2)*, and *OS(3)* for that model will be -2.4, -1.7, and -0.5, respectively.

The component scores GOAP, DFIRE, ITScorePro, ranksum, the LZerD shape score, LZerD cluster size, membrane transfer energy, $OS_{(1)}$, $OS_{(2)}$, and $OS_{(3)}$, were then finally combined in the bagged estimator. Bagging is an ensemble method which constructs multiple estimators using subsets of the training data, and then averages their individual outputs to produce a more robust classifier [67]. To optimize the bagged ensemble, docked models were generated for each target in the training dataset using the same procedure as above. CAPRI statistics were then calculated for each model. Each model was labeled positive if it was of acceptable CAPRI quality, and negative if it was not. Each model was then weighted to balance the number of positive and negative cases within each target. Then, the bagged estimator was trained using all the models for all the training targets. The resulting scoring function, with ranksum component scores used to break ties, was used to rescore the docked models after the clustering stage.

FUNDING

This work used Anvil at Purdue University through allocation CIS230021 from the Advanced Cyberinfrastructure Coordination Ecosystem: Services & Support (ACCESS) program, which is supported by National Science Foundation grants #2138259, #2138286, #2138307, #2137603, and #2138296. This work was partly supported by the National Institutes of Health (R01GM123055, R01GM133840, 3R01 GM133840-02S1) and the National Science Foundation (DMS2151678, DBI2003635, CMMI1825941, MCB2146026, and MCB1925643). CC was supported by NIGMS-funded predoctoral fellowship to CC (T32 GM132024). KH was supported by the Science & Engineering Research Board (SERB), Government of

India through the Overseas Visiting Doctoral Fellowship program (OVDF). The contents of this work are solely the responsibility of the authors and do not necessarily represent the official views of the funding agencies.

ACKNOWLEDGEMENTS

The authors are grateful to Information Technology at Purdue, West Lafayette, Indiana for providing computational resources. This publication was made possible with support from the Purdue Institute of Inflammation, Immunology and Infectious Disease (PI4D).

DECLARATIONS OF INTEREST

The authors declare no conflict of interest.

REFERENCES

1. Berman H. M., Battistuz T., Bhat T. N., Bluhm W. F., Bourne P. E., Burkhardt K., et al. (2002). The Protein Data Bank. *Acta Crystallogr D Biol Crystallogr*. **58**, 899-907.
2. Berman H., Henrick K., Nakamura H. (2003). Announcing the worldwide Protein Data Bank. *Nat Struct Biol*. **10**, 980.
3. Peplow M. (2020). Cryo-Electron Microscopy Reaches Resolution Milestone. *ACS Cent Sci*. **6**, 1274-7.
4. Aderinwale T., Christoffer C. W., Sarkar D., Alnabati E., Kihara D. (2020). Computational structure modeling for diverse categories of macromolecular interactions. *Curr Opin Struct Biol*. **64**, 1-8.
5. Mintseris J., Pierce B., Wiehe K., Anderson R., Chen R., Weng Z. (2007). Integrating statistical pair potentials into protein complex prediction. *Proteins*. **69**, 511-20.
6. Dominguez C., Boelens R., Bonvin A. M. (2003). HADDOCK: a protein-protein docking approach based on biochemical or biophysical information. *J Am Chem Soc*. **125**, 1731-7.
7. Kozakov D., Hall D. R., Xia B., Porter K. A., Padhorny D., Yueh C., et al. (2017). The ClusPro web server for protein-protein docking. *Nat Protoc*. **12**, 255-78.
8. Lyskov S., Gray J. J. (2008). The RosettaDock server for local protein-protein docking. *Nucleic Acids Res*. **36**, W233-8.
9. Ritchie D. W., Venkatraman V. (2010). Ultra-fast FFT protein docking on graphics processors. *Bioinformatics*. **26**, 2398-405.
10. Torchala M., Moal I. H., Chaleil R. A., Fernandez-Recio J., Bates P. A. (2013). SwarmDock: a server for flexible protein-protein docking. *Bioinformatics*. **29**, 807-9.

11. de Vries S., Zacharias M. (2013). Flexible docking and refinement with a coarse-grained protein model using ATTRACT. *Proteins*. **81**, 2167-74.
12. Jumper J., Evans R., Pritzel A., Green T., Figurnov M., Ronneberger O., et al. (2021). Highly accurate protein structure prediction with AlphaFold. *Nature*.
13. Evans R., O'Neill M., Pritzel A., Antropova N., Senior A., Green T., et al. (2021). Protein complex prediction with AlphaFold-Multimer. *bioRxiv*. 2021.10.04.463034.
14. Venkatraman V., Yang Y. D., Sael L., Kihara D. (2009). Protein-protein docking using region-based 3D Zernike descriptors. *BMC Bioinformatics*. **10**, 407.
15. Christoffer C., Terashi G., Shin W. H., Aderinwale T., Maddhuri Venkata Subramaniya S. R., Peterson L., et al. (2020). Performance and enhancement of the LZerD protein assembly pipeline in CAPRI 38-46. *Proteins*. **88**, 948-61.
16. Christoffer C., Chen S., Bharadwaj V., Aderinwale T., Kumar V., Hormati M., et al. (2021). LZerD webserver for pairwise and multiple protein-protein docking. *Nucleic Acids Res*. **49**, W359-W65.
17. Christoffer C., Bharadwaj V., Luu R., Kihara D. (2021). LZerD Protein-Protein Docking Webserver Enhanced With de novo Structure Prediction. *Front Mol Biosci*. **8**, 724947.
18. Lensink M. F., Nadzirin N., Velankar S., Wodak S. J. (2020). Modeling protein-protein, protein-peptide, and protein-oligosaccharide complexes: CAPRI 7th edition. *Proteins*. **88**, 916-38.
19. Lensink M. F., Brysbaert G., Nadzirin N., Velankar S., Chaleil R. A. G., Gerguri T., et al. (2019). Blind prediction of homo- and hetero-protein complexes: The CASP13-CAPRI experiment. *Proteins*. **87**, 1200-21.
20. Koukos P. I., Faro I., van Noort C. W., Bonvin A. (2018). A Membrane Protein Complex Docking Benchmark. *J Mol Biol*. **430**, 5246-56.
21. Lensink M. F., Brysbaert G., Mauri T., Nadzirin N., Velankar S., Chaleil R. A. G., et al. (2021). Prediction of protein assemblies, the next frontier: The CASP14-CAPRI experiment. *Proteins*. **89**, 1800-23.
22. Kolbe M., Besir H., Essen L. O., Oesterhelt D. (2000). Structure of the light-driven chloride pump halorhodopsin at 1.8 A resolution. *Science*. **288**, 1390-6.
23. Kouyama T., Kanada S., Takeguchi Y., Narusawa A., Murakami M., Ihara K. (2010). Crystal structure of the light-driven chloride pump halorhodopsin from Natronomonas pharaonis. *J Mol Biol*. **396**, 564-79.
24. Turnbull A. P., Rafferty J. B., Sedelnikova S. E., Slabas A. R., Schierer T. P., Kroon J. T., et al. (2001). Analysis of the structure, substrate specificity, and mechanism of squash glycerol-3-phosphate (1)-acyltransferase. *Structure*. **9**, 347-53.
25. Gulsevin A., Meiler J. (2021). Prediction of amphipathic helix-membrane interactions with Rosetta. *PLoS Comput Biol*. **17**, e1008818.
26. Fuglebakk E., Reuter N. (2018). A model for hydrophobic protrusions on peripheral membrane proteins. *PLoS Comput Biol*. **14**, e1006325.
27. Sutherland M. C., Jarodsky J. M., Ovchinnikov S., Baker D., Kranz R. G. (2018). Structurally Mapping Endogenous Heme in the CcmCDE Membrane Complex for Cytochrome c Biogenesis. *J Mol Biol*. **430**, 1065-80.
28. Gao M., Nakajima An D., Parks J. M., Skolnick J. (2022). AF2Complex predicts direct physical interactions in multimeric proteins with deep learning. *Nat Commun*. **13**, 1744.
29. Wu R., Bakelar J. W., Lundquist K., Zhang Z., Kuo K. M., Ryoo D., et al. (2021). Plasticity within the barrel domain of BamA mediates a hybrid-barrel mechanism by BAM. *Nat Commun*. **12**, 7131.
30. Alford R. F., Koehler Leman J., Weitzner B. D., Duran A. M., Tilley D. C., Elazar A., et al. (2015). An Integrated Framework Advancing Membrane Protein Modeling and Design. *PLoS Comput Biol*. **11**, e1004398.
31. Hurwitz N., Wolfson H. J. (2021). Memdock: An alpha-Helical Membrane Protein Docking Algorithm. *Methods Mol Biol*. **2315**, 111-7.

32. Hurwitz N., Schneidman-Duhovny D., Wolfson H. J. (2016). Memdock: an alpha-helical membrane protein docking algorithm. *Bioinformatics*. **32**, 2444-50.
33. Rudden L. S. P., Degiacomi M. T. (2021). Transmembrane Protein Docking with JabberDock. *J Chem Inf Model*. **61**, 1493-9.
34. Christoffer C., Kihara D. (2022). Domain-Based Protein Docking with Extremely Large Conformational Changes. *J Mol Biol*. **434**, 167820.
35. Christoffer C., Kihara D. (2022). Modeling protein-nucleic acid complexes with extremely large conformational changes using Flex-LZerD. *Proteomics*. e2200322.
36. Peterson L. X., Roy A., Christoffer C., Terashi G., Kihara D. (2017). Modeling disordered protein interactions from biophysical principles. *PLoS Comput Biol*. **13**, e1005485.
37. Wolfson H. J., Rigoutsos I. (1997). Geometric hashing: An overview. *IEEE computational science and engineering*. **4**, 10-21.
38. Canterakis N. 3D Zernike moments and Zernike affine invariants for 3D image analysis and recognition. In 11th Scandinavian Conf on Image Analysis: Citeseer; 1999.
39. Aderinwale T., Bharadwaj V., Christoffer C., Terashi G., Zhang Z., Jahandideh R., et al. (2022). Real-time structure search and structure classification for AlphaFold protein models. *Commun Biol*. **5**, 316.
40. Shin W. H., Christoffer C. W., Wang J., Kihara D. (2016). PL-PatchSurfer2: Improved Local Surface Matching-Based Virtual Screening Method That Is Tolerant to Target and Ligand Structure Variation. *J Chem Inf Model*. **56**, 1676-91.
41. Esquivel-Rodriguez J., Xiong Y., Han X., Guang S., Christoffer C., Kihara D. (2015). Navigating 3D electron microscopy maps with EM-SURFER. *BMC Bioinformatics*. **16**, 181.
42. Xiong Y., Esquivel-Rodriguez J., Sael L., Kihara D. (2014). 3D-SURFER 2.0: web platform for real-time search and characterization of protein surfaces. *Methods Mol Biol*. **1137**, 105-17.
43. La D., Esquivel-Rodriguez J., Venkatraman V., Li B., Sael L., Ueng S., et al. (2009). 3D-SURFER: software for high-throughput protein surface comparison and analysis. *Bioinformatics*. **25**, 2843-4.
44. Lomize A. L., Todd S. C., Pogozheva I. D. (2022). Spatial arrangement of proteins in planar and curved membranes by PPM 3.0. *Protein Sci*. **31**, 209-20.
45. Lomize M. A., Pogozheva I. D., Joo H., Mosberg H. I., Lomize A. L. (2012). OPM database and PPM web server: resources for positioning of proteins in membranes. *Nucleic Acids Res*. **40**, D370-6.
46. Lee J., Cheng X., Swails J. M., Yeom M. S., Eastman P. K., Lemkul J. A., et al. (2016). CHARMM-GUI Input Generator for NAMD, GROMACS, AMBER, OpenMM, and CHARMM/OpenMM Simulations Using the CHARMM36 Additive Force Field. *J Chem Theory Comput*. **12**, 405-13.
47. Feng L., Yan H., Wu Z., Yan N., Wang Z., Jeffrey P. D., et al. (2007). Structure of a site-2 protease family intramembrane metalloprotease. *Science*. **318**, 1608-12.
48. Brown M. S., Ye J., Rawson R. B., Goldstein J. L. (2000). Regulated intramembrane proteolysis: a control mechanism conserved from bacteria to humans. *Cell*. **100**, 391-8.
49. Zimmermann L., Stephens A., Nam S. Z., Rau D., Kubler J., Lozajic M., et al. (2018). A Completely Reimplemented MPI Bioinformatics Toolkit with a New HHpred Server at its Core. *J Mol Biol*. **430**, 2237-43.
50. Nie L., Pascoa T. C., Pike A. C. W., Bushell S. R., Quigley A., Ruda G. F., et al. (2021). The structural basis of fatty acid elongation by the ELOVL elongases. *Nat Struct Mol Biol*. **28**, 512-20.
51. Zhang K., Kniazeva M., Han M., Li W., Yu Z., Yang Z., et al. (2001). A 5-bp deletion in ELOVL4 is associated with two related forms of autosomal dominant macular dystrophy. *Nat Genet*. **27**, 89-93.
52. Cadieux-Dion M., Turcotte-Gauthier M., Noreau A., Martin C., Meloche C., Gravel M., et al. (2014). Expanding the clinical phenotype associated with ELOVL4 mutation: study of a large French-Canadian family with autosomal dominant spinocerebellar ataxia and erythrokeratodermia. *JAMA Neurol*. **71**, 470-5.

53. Di Gregorio E., Borroni B., Giorgio E., Lacerenza D., Ferrero M., Lo Buono N., et al. (2014). ELOVL5 mutations cause spinocerebellar ataxia 38. *Am J Hum Genet*. **95**, 209-17.
54. Svensson-Ek M., Abramson J., Larsson G., Tornroth S., Brzezinski P., Iwata S. (2002). The X-ray crystal structures of wild-type and EQ(I-286) mutant cytochrome c oxidases from Rhodobacter sphaeroides. *J Mol Biol*. **321**, 329-39.
55. Spencer A. G., Woods J. W., Arakawa T., Singer, II, Smith W. L. (1998). Subcellular localization of prostaglandin endoperoxide H synthases-1 and -2 by immunoelectron microscopy. *J Biol Chem*. **273**, 9886-93.
56. Duggan K. C., Walters M. J., Musee J., Harp J. M., Kiefer J. R., Oates J. A., et al. (2010). Molecular basis for cyclooxygenase inhibition by the non-steroidal anti-inflammatory drug naproxen. *J Biol Chem*. **285**, 34950-9.
57. Hogestatt E. D., Jonsson B. A., Ermund A., Andersson D. A., Bjork H., Alexander J. P., et al. (2005). Conversion of acetaminophen to the bioactive N-acylphenolamine AM404 via fatty acid amide hydrolase-dependent arachidonic acid conjugation in the nervous system. *J Biol Chem*. **280**, 31405-12.
58. Rowlinson S. W., Kiefer J. R., Prusakiewicz J. J., Pawlitz J. L., Kozak K. R., Kalgutkar A. S., et al. (2003). A novel mechanism of cyclooxygenase-2 inhibition involving interactions with Ser-530 and Tyr-385. *J Biol Chem*. **278**, 45763-9.
59. Kurumbail R. G., Stevens A. M., Gierse J. K., McDonald J. J., Stegeman R. A., Pak J. Y., et al. (1996). Structural basis for selective inhibition of cyclooxygenase-2 by anti-inflammatory agents. *Nature*. **384**, 644-8.
60. Eydoux C., De Caro J., Ferrato F., Boullanger P., Lafont D., Laugier R., et al. (2007). Further biochemical characterization of human pancreatic lipase-related protein 2 expressed in yeast cells. *J Lipid Res*. **48**, 1539-49.
61. van Bennekum A. M., Fisher E. A., Blaner W. S., Harrison E. H. (2000). Hydrolysis of retinyl esters by pancreatic triglyceride lipase. *Biochemistry*. **39**, 4900-6.
62. van Tilbeurgh H., Egloff M. P., Martinez C., Rugani N., Verger R., Cambillau C. (1993). Interfacial activation of the lipase-procolipase complex by mixed micelles revealed by X-ray crystallography. *Nature*. **362**, 814-20.
63. Steinegger M., Soding J. (2018). Clustering huge protein sequence sets in linear time. *Nat Commun*. **9**, 2542.
64. Mukherjee S., Zhang Y. (2009). MM-align: a quick algorithm for aligning multiple-chain protein complex structures using iterative dynamic programming. *Nucleic Acids Res*. **37**, e83.
65. Esquivel-Rodriguez J., Filos-Gonzalez V., Li B., Kihara D. (2014). Pairwise and multimeric protein-protein docking using the LZerD program suite. *Methods Mol Biol*. **1137**, 209-34.
66. Arya S., Mount D. M., Netanyahu N. S., Silverman R., Wu A. Y. (1998). An optimal algorithm for approximate nearest neighbor searching fixed dimensions. *J ACM*. **45**, 891–923.
67. Breiman L. (1996). Bagging predictors. *Machine Learning*. **24**, 123-40.
68. Zhou H., Skolnick J. (2011). GOAP: a generalized orientation-dependent, all-atom statistical potential for protein structure prediction. *Biophys J*. **101**, 2043-52.
69. Zhou H., Zhou Y. (2002). Distance-scaled, finite ideal-gas reference state improves structure-derived potentials of mean force for structure selection and stability prediction. *Protein Sci*. **11**, 2714-26.
70. Huang S. Y., Zou X. (2011). Statistical mechanics-based method to extract atomic distance-dependent potentials from protein structures. *Proteins*. **79**, 2648-61.
71. Peterson L. X., Kim H., Esquivel-Rodriguez J., Roy A., Han X., Shin W. H., et al. (2017). Human and server docking prediction for CAPRI round 30-35 using LZerD with combined scoring functions. *Proteins*. **85**, 513-27.

72. Peterson L. X., Shin W. H., Kim H., Kihara D. (2018). Improved performance in CAPRI round 37 using LZerD docking and template-based modeling with combined scoring functions. *Proteins*. **86 Suppl 1**, 311-20.
73. MacCallum J. L., Bennett W. F., Tieleman D. P. (2007). Partitioning of amino acid side chains into lipid bilayers: results from computer simulations and comparison to experiment. *J Gen Physiol*. **129**, 371-7.